Biomedical Optics EXPRESS

Surface modification of silica particles with gold nanoparticles as an augmentation of gold nanoparticle mediated laser perforation

Stefan Kalies,[1,*] Lara Gentemann,[1] Markus Schomaker,[1] Dag Heinemann,[1] Tammo Ripken,[1] and Heiko Meyer[1,2]

[1]*Biomedical Optics Department, Laser Zentrum Hannover e.V., Hollerithallee 8, 30419 Hannover, Germany*
[2]*Department of Cardiothoracic, Transplantation and Vascular Surgery, Hannover Medical School, Carl-Neuberg-Straße 1, 30625 Hannover, Germany*
[*]*s.kalies@lzh.de*

Abstract: Gold nanoparticle mediated (GNOME) laser transfection/perforation fulfills the demands of a reliable transfection technique. It provides efficient delivery and has a negligible impact on cell viability. Furthermore, it reaches high-throughput applicability. However, currently only large gold particles (> 80 nm) allow successful GNOME laser perforation, probably due to insufficient sedimentation of smaller gold nanoparticles. The objective of this study is to determine whether this aspect can be addressed by a modification of silica particles with gold nanoparticles. Throughout the analysis, we show that after the attachment of gold nanoparticles to silica particles, comparable or better efficiencies to GNOME laser perforation are reached. In combination with 1 µm silica particles, we report laser perforation with gold nanoparticles with sizes down to 4 nm. Therefore, our investigations have great importance for the future research in and the fields of laser transfection combined with plasmonics.

OCIS codes: (350.4855) Optical tweezers or optical manipulation; (000.1430) Biology and medicine; (160.4236) Nanomaterials; (350.4990) Particles.

References and links

1. K. A. Whitehead, R. Langer, and D. G. Anderson, "Knocking down barriers: advances in siRNA delivery," Nat. Rev. Drug Discov. **8**(2), 129–138 (2009).
2. A. de Fougerolles, H.-P. Vornlocher, J. Maraganore, and J. Lieberman, "Interfering with disease: a progress report on siRNA-based therapeutics," Nat. Rev. Drug Discov. **6**(6), 443–453 (2007).
3. K. Gao and L. Huang, "Nonviral methods for siRNA delivery," Mol. Pharm. **6**(3), 651–658 (2009).
4. T. M. Allen and P. R. Cullis, "Liposomal drug delivery systems: from concept to clinical applications," Adv. Drug Deliv. Rev. **65**(1), 36–48 (2013).
5. J. Piñero, M. López-Baena, T. Ortiz, and F. Cortés, "Apoptotic and necrotic cell death are both induced by electroporation in HL60 human promyeloid leukaemia cells," Apoptosis **2**(3), 330–336 (1997).
6. J. Panyam and V. Labhasetwar, "Biodegradable nanoparticles for drug and gene delivery to cells and tissue," Adv. Drug Deliv. Rev. **55**(3), 329–347 (2003).
7. N. L. Rosi, D. A. Giljohann, C. S. Thaxton, A. K. Lytton-Jean, M. S. Han, and C. A. Mirkin, "Oligonucleotide-modified gold nanoparticles for intracellular gene regulation," Science **312**(5776), 1027–1030 (2006).
8. I. I. Slowing, J. L. Vivero-Escoto, C.-W. Wu, and V. S.-Y. Lin, "Mesoporous silica nanoparticles as controlled release drug delivery and gene transfection carriers," Adv. Drug Deliv. Rev. **60**(11), 1278–1288 (2008).
9. C. Kneuer, M. Sameti, U. Bakowsky, T. Schiestel, H. Schirra, H. Schmidt, and C.-M. Lehr, "A Nonviral DNA Delivery System Based on Surface Modified Silica-Nanoparticles Can Efficiently Transfect Cells in Vitro," Bioconjug. Chem. **11**(6), 926–932 (2000).
10. M. Tsukakoshi, S. Kurata, Y. Nomiya, Y. Ikawa, and T. Kasuya, "A novel method of DNA transfection by laser microbeam cell surgery," Appl. Phys. B. **35**(3), 135–140 (1984).
11. U. K. Tirlapur, K. König, C. Peuckert, R. Krieg, and K. J. Halbhuber, "Femtosecond near-infrared laser pulses elicit generation of reactive oxygen species in mammalian cells leading to apoptosis-like death," Exp. Cell Res. **263**(1), 88–97 (2001).
12. D. J. Stevenson, F. J. Gunn-Moore, P. Campbell, and K. Dholakia, "Single cell optical transfection," J. R. Soc. Interface **7**(47), 863–871 (2010).

#211586 - $15.00 USD Received 13 May 2014; revised 26 Jun 2014; accepted 27 Jun 2014; published 17 Jul 2014

13. A. Vogel, J. Noack, G. Hüttman, and G. Paltauf, "Mechanisms of femtosecond laser nanosurgery of cells and tissues," Appl. Phys. B **81**(8), 1015–1047 (2005).
14. J. Baumgart, L. Humbert, É. Boulais, R. Lachaine, J.-J. Lebrun, and M. Meunier, "Off-resonance plasmonic enhanced femtosecond laser optoporation and transfection of cancer cells," Biomaterials **33**(7), 2345–2350 (2012).
15. D. Heinemann, M. Schomaker, S. Kalies, M. Schieck, R. Carlson, H. M. Escobar, T. Ripken, H. Meyer, and A. Heisterkamp, "Gold nanoparticle mediated laser transfection for efficient siRNA mediated gene knock down," PLoS ONE **8**(3), e58604 (2013).
16. S. Kalies, D. Heinemann, M. Schomaker, H. M. Escobar, A. Heisterkamp, T. Ripken, and H. Meyer, "Plasmonic laser treatment for Morpholino oligomer delivery in antisense applications," J. Biophoton. doi: 10.1002/jbio.201300056. (2013)
17. S. Kalies, T. Birr, D. Heinemann, M. Schomaker, T. Ripken, A. Heisterkamp, and H. Meyer, "Enhancement of extracellular molecule uptake in plasmonic laser perforation," J. Biophoton. doi: 10.1002/jbio.201200200, (2013).
18. G. Bisker and D. Yelin, "Noble-metal nanoparticles and short pulses for nanomanipulations: theoretical analysis," J. Opt. Soc. Am. B **29**(6), 1383 (2012).
19. E. Boulais, R. Lachaine, and M. Meunier, "Plasma mediated off-resonance plasmonic enhanced ultrafast laser-induced nanocavitation," Nano Lett. **12**(9), 4763–4769 (2012).
20. C. Yao, X. Qu, Z. Zhang, G. Hüttmann, and R. Rahmanzadeh, "Influence of laser parameters on nanoparticle-induced membrane permeabilization," J. Biomed. Opt. **14**(5), 054034 (2009).
21. E. Y. Lukianova-Hleb, X. Ren, P. E. Constantinou, B. P. Danysh, D. L. Shenefelt, D. D. Carson, M. C. Farach-Carson, V. A. Kulchitsky, X. Wu, D. S. Wagner, and D. O. Lapotko, "Improved cellular specificity of plasmonic nanobubbles versus nanoparticles in heterogeneous cell systems," PLoS ONE **7**(4), e34537 (2012).
22. N. R. Jana, L. Gearheart, and C. J. Murphy, "Wet Chemical Synthesis of High Aspect Ratio Cylindrical Gold Nanorods," J. Phys. Chem. B **105**(19), 4065–4067 (2001).
23. S. Westcott, S. Oldenburg, T. Lee, and N. Halas, "Formation and adsorption of clusters of gold nanoparticles onto functionalized silica nanoparticle surfaces," Langmuir **14**(19), 5396–5401 (1998).
24. S. L. Voytik-Harbin, A. O. Brightman, B. Waisner, C. H. Lamar, and S. F. Badylak, "Application and evaluation of the alamarBlue assay for cell growth and survival of fibroblasts," In Vitro Cell. Dev. Biol. Anim. **34**(3), 239–246 (1998).
25. P. Laven, "MiePlot: a computer program for scattering of light from a sphere using Mie theory & the Debye series," *http://www.philiplaven.com/mieplot.htm*
26. A. Vogel and V. Venugopalan, "Mechanisms of pulsed laser ablation of biological tissues," Chem. Rev. **103**(2), 577–644 (2003), doi:10.1021/cr010379n.
27. C. Liu, Z. Li, and Z. Zhang, "Mechanisms of laser nanoparticle-based techniques for gene transfection-a calculation study," J. Biol. Phys. **35**(2), 175–183 (2009).
28. H. Goldenberg and C. J. Tranter, "Heat flow in an infinite medium heated by a sphere," Br. J. Appl. Phys. **3**(9), 296–298 (1952).
29. C. A. Schneider, W. S. Rasband, and K. W. Eliceiri, "NIH Image to ImageJ: 25 years of image analysis," Nat. Methods **9**(7), 671–675 (2012).
30. J. Neumann and R. Brinkmann, "Boiling nucleation on melanosomes and microbeads transiently heated by nanosecond and microsecond laser pulses," J. Biomed. Opt. **10**(2), 024001 (2005).
31. V. P. Zharov, R. R. Letfullin, and E. N. Galitovskaya, "Microbubbles-overlapping mode for laser killing of cancer cells with absorbing nanoparticle clusters," J. Phys. D Appl. Phys. **38**(15), 2571–2581 (2005).
32. I. M. M. Paino, V. S. Marangoni, R. C. de Oliveira, L. M. G. Antunes, and V. Zucolotto, "Cyto and genotoxicity of gold nanoparticles in human hepatocellular carcinoma and peripheral blood mononuclear cells," Toxicol. Lett. **215**(2), 119–125 (2012).
33. M. Tsoli, H. Kuhn, W. Brandau, H. Esche, and G. Schmid, "Cellular uptake and toxicity of Au55 clusters," Small **1**(8-9), 841–844 (2005).

1. Introduction

The development of novel therapeutic applications includes the research on the delivery of small interfering RNA (siRNA), proteins and peptides, or DNA [1]. In particular, siRNA is of great interest. It is capable of inducing a knockdown of the expression of a gene of interest [1, 2]. A crucial step is the delivery of sufficient siRNA levels into cells [1–3]. There are biochemical or physical strategies for the transfection of siRNA into cells. In liposomal delivery, the negatively charged siRNA forms an aggregate with a cationic lipid [4]. This is taken up through the negatively charged phospholipid bilayer. Electroporation, as a physical method, is also well suited for the highly efficient delivery of genetic material into cells. However, the cells are exposed to an electric pulse for micro- to milliseconds, which decreases cell viability [5]. In the last two decades, new, alternative transfection techniques to these common methods have been developed.

Nanoparticle based transfection represents an alternative to common transfection techniques [6–9]. It utilizes nanoparticles of different material, shape and size. Biodegradable

#211586 - $15.00 USD Received 13 May 2014; revised 26 Jun 2014; accepted 27 Jun 2014; published 17 Jul 2014

poly(lactic-co-glycolic acid) nanoparticles enable the delivery of various agents [6]. Another example for this purpose is the use of gold nanoparticles as demonstrated by Rosi et al. [7]. Silica particles are an additional alternative for the delivery of genetic material into cells. As an example, either cationic silica nanoparticles or mesoporous silica nanoparticles are able to release genetic material in the cells after uptake [8, 9].

An important physical approach for transfection is the utilization of laser irradiation to achieve a transient membrane permeabilization [10–12]. This enables the inflow of the genetic material of interest. It is desirable to reach the transfection of many cells on a short time scale. This high-throughput applicability is not reached by most laser transfection techniques. Many of them make use of laser spots focused onto the membrane of a single cell [10–12]. In the case of femtosecond laser pulses, this induces the formation of a low electron density plasma by the ionization of water and biomolecules [8, 12]. Thereby, the cell membrane is permeabilized and extracellular molecules can cross it. While this holds the advantage of single cell selectivity, it cannot reach the desired high-throughput [13].

As a combination of nanoparticle and laser based transfection, the delivery of genetic material after laser irradiation of plain spherical gold nanoparticles on the cell membrane was shown recently [14–17]. Gold nanoparticle mediated laser transfection is possible with femtosecond irradiation in the near infrared range. A functional model developed by our group utilizes a picosecond laser at a wavelength of 532 nm. Irradiation of the gold nanoparticles causes either permeabilization by near-field enhancement with nanocavitation or by heating of the gold nanoparticles [17, 18]. Both depend on the laser parameters, in particular pulse length and wavelength. Additionally, biological and particle parameters, such as size and shape, need to be considered [16–20]. Only antibody or peptide conjugated particles enable cell selectivity [20].

As a third parameter set, the permeabilization can be influenced by the state of the gold nanoparticles on the cell. Lukianova-Hleb et al. reported permeabilization with gold nanoparticles, which were taken up by the cells, and formed clusters [21]. Our group showed that gold nanoparticles attached to the cellular membrane are sufficient to induce the same effects [15]. For the end user, short incubation times are highly desirable, but this is restricted by the particle sedimentation. Up to now, only large plain particles (> 80 nm) were applied for successful delivery of siRNA, Morpholinos or DNA [14–17]. This is probably due to negligible sedimentation and unspecific cell attachment for smaller particles, especially if they are not conjugated with antibodies as in the case of Yao et al. [16, 20]. Next to this, the particles size, and the inter particle distance are of great importance, because both influence the spatial interaction zone. Single particles with a distance of one or two micrometers might cause two separate loci of permeabilization. Two nanoparticles with a short distance could possibly cause a single, merged locus. The sizes of the nanoparticles correspond to different absorption efficiencies. Therefore, particles of other sizes than the routinely used large particles might also enhance perforation.

It would be highly desirable to explore how the use of small particles down to a few nanometers can be addressed. In order to guarantee routine usage, this ought to be achieved without the conjugation to antibodies, because this would require appropriate epitopes on the cell membrane [20]. Furthermore, it would be of great interest to keep the distance between two particles short without overall high concentrations of nanoparticles on the cell membrane. This might lead to spatial heat overlapping zones and increase perforation efficiency.

We determined that gold nanoparticle binding to surface modified silica particles could be well suited to address these issues. We used silica microparticles of 1 μm in size which should sediment on sufficiently shorter time scales before perforation. Furthermore, due to their large size, the uptake of these particles is less likely. Gold nanoparticles of sizes 4 nm, 15 nm, and 30 nm were bound to the silica particles. For larger particles, the ratio of silica microparticles to gold nanoparticles is no longer interesting because of the desired nanoparticle and surface concentration (see Table 1). While 4 nm particles only show low absorption, the absorption of 30 nm compared to the routinely used 200 nm particles is

#211586 - $15.00 USD Received 13 May 2014; revised 26 Jun 2014; accepted 27 Jun 2014; published 17 Jul 2014

higher. Throughout the analysis, comparable or better efficiencies to the previous GNOME laser perforation technique were reached.

2. Methods and materials

2.1. Experimental setup

The perforation system used in this study was described previously [15]. Briefly, the laser system operates at a wavelength of 532 nm. The Nd:YAG Microchip laser (Horus, France) generates pulses of 850 ps at a repetition rate of 20.25 kHz. A telescope adjusts the beam diameter and a combination of a half-wave plate and a polarizing beam splitter cube serves to attenuate the power. Two galvanometer scanning mirrors and a focusing lens enable to scan each sample with a meandering pattern. The radiant exposure was fixed to 42 mJ/cm^2 and the scanning velocity was set to 200 mm/s. This proved to be the best combination in our previous studies [15–17]. It enables to perforate about 60,000 cells within 8 seconds. Heinemann et al. give a more detailed description of the parameters [15].

2.2. Preparation of gold nanoparticle modified silica particles

Spherical unconjugated gold nanoparticles of 15 nm and 30 nm diameter (PGO15 and PGO30, Kisker Biotech, Germany) were used as delivered with a stock concentration of about 0.06 mg/ml. 4 nm gold nanoparticles were prepared by the reduction of gold salt (Gold(III) chloride trihydrate (Sigma, Germany) through sodium borohydride (Sigma) in the presence of trisodium citrate (Carl Roth, Germany) as described elsewhere [22].

Plain fluorescent red silica particles (fluo-red) of the size 1 µm (PSi-R1.0, Kisker Biotech, Germany) were used with a stock concentration of 50 mg/ml. These were treated with 1% (3-Aminopropyl)trimethoxysilane (Sigma, Germany) for 15 min. Then, 4.8e8 silica particles (10 µl) were taken and mixed with different concentrations of gold nanoparticles. The approximate gold nanoparticle count per single silica microparticle is given in Table 1. The different ratios (1:10, 1:20, and 1:40) primarily represent the different volume concentrations of silica particles and gold nanoparticles which were used in mixing. Therefore, a ratio of 1:10 means that one part silica particles (e.g. 10 µl) were mixed with nine parts of the gold nanoparticle stock solution (e.g. 90 µl). This led to different amounts of gold nanoparticles per single silica particle for different ratios and particle sizes, respectively (see Fig. 1 for an example). Throughout the following sections, we use the volume-ratio as abbreviation for the used particle set.

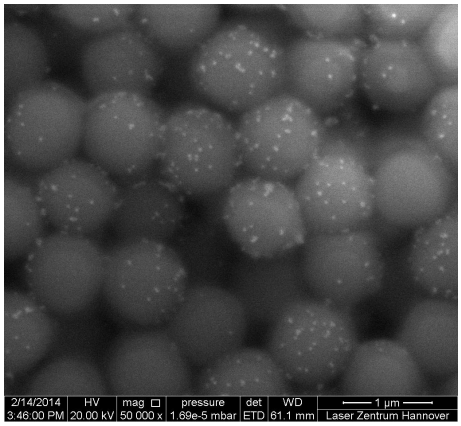

Fig. 1. Binding of 30 nm particles to 1µm silica microparticles at the highest ratio of 1:40. Some particles formed clusters and are in very close distance. The image is recorded with electron microscopy (Quanta 400F, FEI, Netherlands).

#211586 - $15.00 USD Received 13 May 2014; revised 26 Jun 2014; accepted 27 Jun 2014; published 17 Jul 2014

Table 1. Number of gold nanoparticles per single silica particle for the indicated volumetric ratios depending on the size of gold nanoparticles and on the ratio of the mixed silica and gold nanoparticle stock solutions.

nanoparticle size/ volumetric ratio	1:10	1:20	1:40
4 nm gold nanoparticles	9,400	19,800	40,600
15 nm gold nanoparticles	260	550	1,140
30 nm gold nanoparticles	40	80	160

Within 15 min, binding of the gold nanoparticles to the silica particles was clearly visible due to sedimentation. The gold nanoparticle modified silica particles were centrifuged at 400 g for 5 min and dispersed in an equal amount of water for all ratios. The stock solution had a mass concentration of 5 mg/ml. A detailed study on the binding of gold to silica particles and the mechanisms is available by Westcott et al. [23].

2.3 Preparation of cells and perforation procedure

Canine adenoma ZMTH3 cells were cultured in RPMI 1640 medium (Biochrom, Germany) supplemented with 10% fetal calf serum and 1% of the antibiotics penicillin and streptomycin at 37°C and 5% humidified CO2 atmosphere. Laser treatment of the cells was performed in RPMI 1640 at room temperature. One day before the experiments, 30,000 ZMTH3 cells were seeded in black 96-well clear-bottom plates (Corning GmbH, Germany) suitable for fluorescence measurements. All experiments were performed at three independent points in time. At each point in time, the experiments were conducted in three technical replicates.

- *Perforation with free gold nanoparticles (standard procedure):* Usually the perforation with GNOME laser transfection is performed with 200 nm spherical unconjugated gold nanoparticles (PGO200, Kisker Biotech). They proved to be best suited for GNOME laser perforation compared to nanoparticles with sizes down to 80 nm, possibly due to fast sedimentation [16]. In all experimental settings which used only 200 nm gold nanoparticles without silica, these particles were added to the cells 3 hours prior to laser treatment [15–17]. In a previous study we showed, that a nanoparticle mass concentration of 0.5 µg/cm^2 corresponded to approximately six particles per cell in an about 90% confluent 96-well plate well [15]. Compared to this, the calculated amount of nanoparticles per cell is approximately 30 for this concentration based on about 60,000 cells per well and a growth surface area of 0.35 cm^2.
- *Perforation with combined gold nanoparticle - silica particles (enhanced procedure):* The perforation with gold nanoparticle modified silica particles (termed "silica-GNP-particles") was carried out as follows. The ready-prepared particles in water were mixed with the perforation medium and added to the cells 30 min before laser treatment. This time was found to be sufficient in a prior experiment (see section 3.2). Two mass concentrations were applied. A concentration of 2 µg/cm^2 of silica-GNP-particles corresponded to a calculated amount of approximately 10 particles per cell, while a concentration of 20 µg/cm^2 was about 100 particles per cell. Even a high ratio of gold nanoparticles to silica particles does not alter the mass ratio severely. In the case of the highest amount of gold nanoparticles binding to a single silica particle, the mass of the silica particle is about two magnitudes higher than the mass of all gold nanoparticles. Therefore, the number of gold nanoparticles binding to a single silica particle does not affect sedimentation.

2.4 Readout of perforation efficiency and cell viability

Fluorescein isothiocyanate (FITC) labeled dextrans of the size 10 kDa (FD-10S, Sigma) were used to assess the delivery efficiency of the proposed method. These represent siRNA delivery very well as we could show in our previous studies [15]. The dextrans were dissolved in phosphate buffered saline at a concentration of 20 mg/mL and diluted 1:10 in RPMI 1640 for the experiments. FITC fluorescence was measured with the infinite 200 Pro

#211586 - $15.00 USD Received 13 May 2014; revised 26 Jun 2014; accepted 27 Jun 2014; published 17 Jul 2014

plate reader (Tecan, Switzerland) to obtain a quantitative fluorescence value per well. This resembles a reliable indicator of perforation efficiency [15–17]. An equal number to the laser treated samples remained as non-treated negative control and was substracted in the fluorescence measurements. The build-in monochromator was set to an excitation wavelength of 488 nm ± 9 nm and the emission maximum was 520 nm ± 20 nm. Before the measurement, the cells were washed several times with RPMI 1640 after laser treatment to eliminate any remaining background fluorescence. A fluorescence microscope (Zeiss Axiovert 200, Carl Zeiss, Germany) equipped with an EMCCD-camera (Andor Luca R, Andor, United Kingdom) served to take pictures of the cells.

To obtain the cell viability, the indicator QBlue (BioChain, United States) was added to the cells 1 h after laser treatment. A concentration of 10% v/v was used. After another hour, the fluorescence of resorufin was measured. The excitation wavelength was 570 nm ± 20 nm. The emission wavelength was 600 nm ± 9 nm. Only metabolically active cells yield the fluorescent resorufin after reduction of resazurin (QBlue) [24]. The viability measurements were normalized to the untreated control.

2.5 Calculation of the temperature at the particle

To analyze the experimental results temperature calculations were conducted. To obtain values for the extinction, scattering and absorption efficiency the software MiePlot by Philip Laven was retrieved [25]. Water was treated as surrounding medium [26]. Based on these efficiencies we calculated the temperature rise associated with the irradiation of the particles by a model first presented by Liu et al. [27]. It is based on a heat transfer model developed by Goldenberg and Tranter [28]. This provides the heat transfer of a uniformly heated homogeneous sphere embedded in an infinite homogeneous medium. All temperature calculations were evaluated at the end of the 850 ps laser pulse at 532 nm for the fixed radiant exposure of 42 mJ/cm^2. The temporal temperature decrease was not taken into account.

3. Results and discussion

3.1 Calculation of the temperature rise at a single gold particle

In order to relate the perforation to a physical magnitude, the temperature of a single gold nanoparticle was calculated. The nanospheres were treated as single particles. Binding to the silica particles or clusterization were not analyzed. Furthermore, the repetition rate is 20.25 kHz, therefore accumulation of thermal effects is not considered. The extinction, scattering and absorption efficiency are given (see Table 2).

Table 2. Extinction, scattering and absorption efficiency as well as the calculated temperature rise.

nanoparticle size	4 nm	15 m	30 nm	200 nm
extinction efficiency	0.23	0.90	2.00	4.38
scattering efficiency	1.78E-5	3.63E-3	6.28E-2	2.75
absorption efficiency	0.23	0.90	1.94	1.62
maximal temperature rise [K]	85	903	2607	1335

The maximum temperature rise, occurring at the end of the pulse, is calculated additionally to the progression of the temperature inside and outside of the gold particle (see Fig. 2). Depending on the particle size, the temperature rise drops below 100 K at a few ten nanometers distance away from the surface of the particle.

#211586 - $15.00 USD Received 13 May 2014; revised 26 Jun 2014; accepted 27 Jun 2014; published 17 Jul 2014

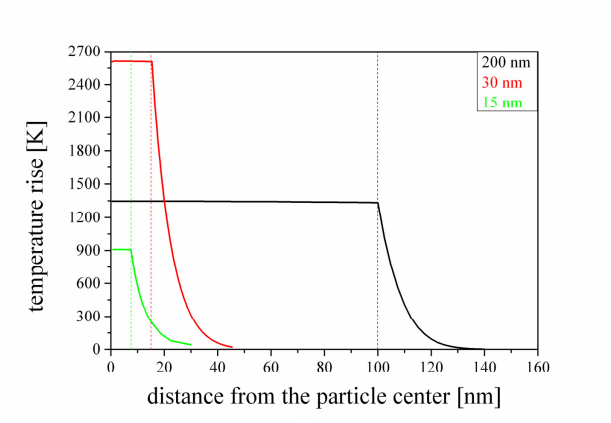

Fig. 2. Progression of the temperature rise inside and outside of spherical gold nanoparticles irradiated with 850 ps laser pulses at a wavelength of 532 nm and a radiant exposure of 42 mJ/cm^2.

Interestingly, in the case of 4 nm particles, the temperature at the surface of a single particle is below the starting point of heterogeneous nucleation. That is more than 200°C [30]. This would exclude a perforation mechanism relying on bubble formation. However, clusterization of the 4 nm particles on the silica particle is likely, what would affect the temperature significantly [23, 31]. The heating zones, and possible bubbles, can overlap, which probably increases the membrane permeabilization.

3.2 Incubation period for silica-gold particles

In respect of our assumption that silica-GNP-particles sediment on short timescales, we first evaluated the amount of silica-GNP-particles per cell 30 min after the start of incubation. For this purpose, we used silica-GNP-particles with a ratio of 1:40 and a gold nanoparticle size of 4 nm. A concentration of 2 µg/cm^2 particles was applied. Cells were co-stained with Calcein-AM green and Hoechst 33342. Red fluorescent particles and cells were counted with ImageJ [27].

In the experiments, a concentration of 7.9 ± 2.3 particles per cell was observed (see Fig. 3(a)). This is in good agreement with the given assumption. As stated in the methods, the number of gold nanoparticles binding to a single silica particle should not affect sedimentation. Hence, the numbers of silica-GNP-particles per cell were treated as equal in the further study, independent of the ratio of gold particles per single silica particle. With a higher silica particle concentration of 20 µg/cm^2, an accumulation of silica-GNP-particles in clusters and stronger levels of particles at the membrane were encountered more often (see Fig. 3(b)). Due to the high particle levels and clustering, it was not possible to give a reliable particle count for this concentration.

#211586 - $15.00 USD Received 13 May 2014; revised 26 Jun 2014; accepted 27 Jun 2014; published 17 Jul 2014

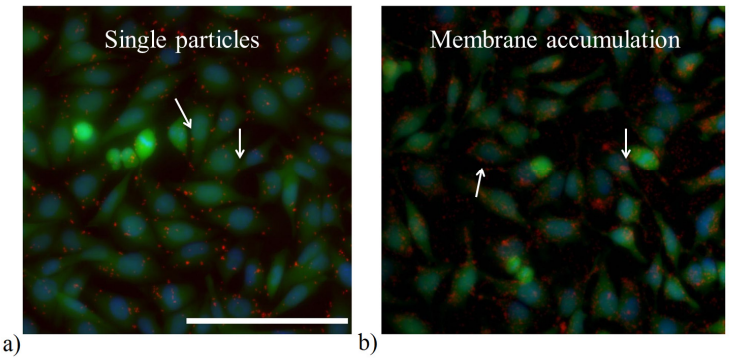

Fig. 3. Microscopic images illustrating the number of particles per cell after 30 min of incubation. Cells are co-stained with Calcein AM green (green) and Hoechst 33342 (blue). Particles are red fluorescent. For a mass concentration of 2 µg/cm^2 about 7.9 ± 2.3 particles per cell were present (a). The higher concentration of silica particles (b) led to an accumulation of particles on the membrane, while the lower concentration yielded separated particles (see arrows). Scale bar 100 µm.

3.3 Optimization of the perforation parameter set

In order to evaluate the best suited particle configuration for the procedure, we tested several combinations and amounts of gold nanoparticles and silica microparticles as described in the methods section. With a surface concentration of 2 µg/cm^2, we gained the best perforation efficiency at a silica particle to gold particle ratio of 1:40 with 15 nm particles (see Fig. 4(a)). For the higher concentration, better fluorescence and perforation values were yielded for 4 nm gold nanoparticles at ratios of 1:20 and 1:40.

Overall, no strong decrease in viability for the lower particle concentration was revealed (see Fig. 4(b)). Compared to this, the higher concentration yielded a decrease in viability to about half of the untreated value after irradiation for gold nanoparticles of 15 nm and 30 nm. In the case of 4 nm gold particles only a slight decrease was observable. In the next experiments, we concentrated on the four best suited parameter sets (1:20 and 1:40 with 4 nm and 100 particles per cell; 1:10 or 1:40 with 15 nm and 100 or 10 particles per cell) which were yielded by this measurement.

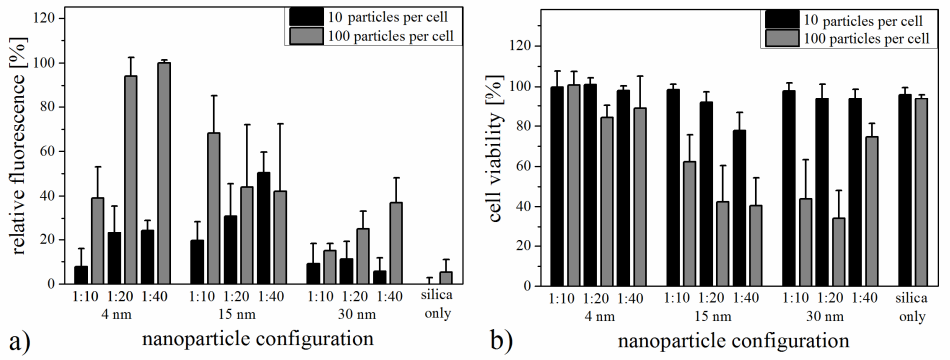

Fig. 4. a) Relative fluorescence of 10 kDa dextrans after laser treatment normalized to the highest level. b) Corresponding cell viability one hour after laser treatment. The highest fluorescence levels for about 10 particles per cell (2 µg/cm^2) were obtained for silica-gold particle ratio of 1:40 for 15 nm particles. For 100 particles per cell (20 µg/cm^2), silica particles modified with 4 nm gold particles yielded the best perforation. In the case of larger particles, the viability was deteriorated to about half of the untreated control. No perforation or decrease in viability was observed for unmodified silica particles.

#211586 - $15.00 USD Received 13 May 2014; revised 26 Jun 2014; accepted 27 Jun 2014; published 17 Jul 2014

The different gold particle sizes or concentrations imply different surface coverage of the silica particle. The distance between two particles is shortened with the higher amount of gold nanoparticles (see Table 1). Furthermore, the absorption efficiency and the associated maximal temperature rise vary for different nanoparticle sizes (see Table 2 and Fig. 2). This explains the different perforation efficiencies and cell viabilities. The cell viability with about 100 silica particles per cell is worst for 30 nm particles. This can be caused by the formation of too many loci of intense heating. In the case of 4 nm particles, the heating is less pronounced. Therefore the viability is higher with this concentration. With 10 particles per cell, the number of gold particles per cell, which are located on the membrane, is probably too low for 30 nm particles. For this reason, the perforation efficiency is lower compared to 15 nm and 4 nm particles. The absorption and temperature rise of the 15 nm particles is higher than for the 4 nm particles. This can yield the better perforation with 10 particles per cell (see Fig. 4).

3.4 Comparison to the standard procedure of GNOME laser perforation

In the next step, we compared the best parameters from the previous section to gold nanoparticle mediated laser perforation with the standard procedure of 3 h incubation and 200 nm particles at 0.5 µg/cm^2 [15]. All analyzed samples showed better perforation efficiencies than the standard procedure (see Fig. 5(a) and 6). A two-fold increase was found for the three parameters using 100 particles per cell. In the case of about 10 silica-GNP-particles, which is comparable to the six gold nanoparticles per cell in the standard procedure, a fluorescence increase of about 50% was observed. Controls which were only laser irradiated or controls with silica particles and irradiation showed no perforation. The viability was only slightly affected after the procedure (see Fig. 5(b)). A group of controls, that was not irradiated, but contained particles, showed slightly higher viabilities than the appropriate irradiated samples. Therefore, the particles do not show any strong cytotoxic effects. Microscopic analysis underlined the examinations concerning the perforation efficiency (see Fig. 6).

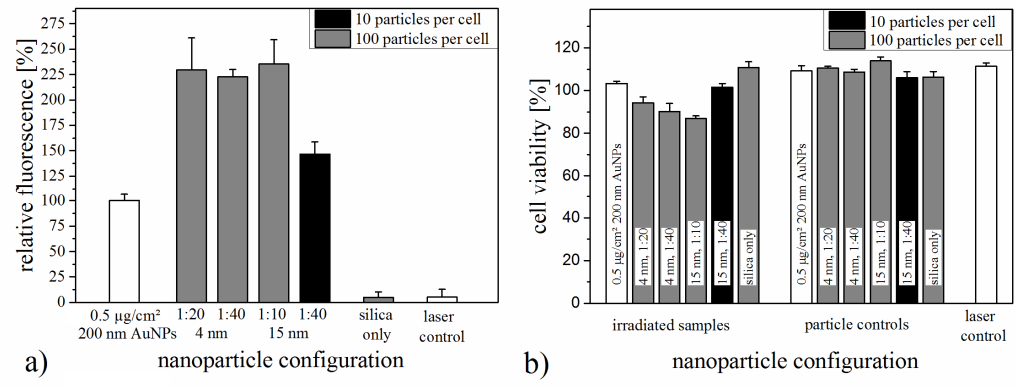

Fig. 5. a) Relative fluorescence of 10 kDa dextrans after laser treatment normalized to the level of gold nanoparticle mediated laser perforation using 200 nm gold nanoparticles and the standard procedure of 3 hours of incubation (~six particles per cell, 0.5 µg/cm^2). b) Corresponding cell viability one hour after laser treatment. The level of fluorescence is increased for the procedure employing the gold modified silica particles. Hence, the perforation efficiency, combining total fluorescence and fluorescence per cell, is higher. The viability is slightly lower compared to the standard procedure. It is not affected by the particles itself, as no impact on the particle controls was observable.

#211586 - $15.00 USD Received 13 May 2014; revised 26 Jun 2014; accepted 27 Jun 2014; published 17 Jul 2014

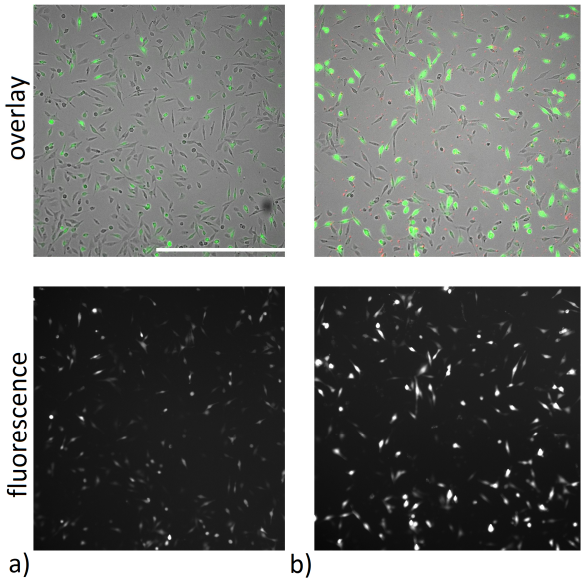

Fig. 6. Microscopic images illustrating perforation with 10 kDa dextrans. In a) the perforation efficiency with 200 nm gold nanoparticles after 3h of incubation is depicted, while b) demonstrates the perforation efficiency with 15 nm silica-GNP-particles at a ratio of 1:40. The efficiency, which combines the number of fluorophores per cell and the totally perforated cell number with our readout, is slightly higher for the silica-GNP-particles. Scale bar 500 µm.

The main differences to the standard procedure are the particle localization and particle size. The application of free gold nanoparticles leads to a random distribution over the cell surface. This causes independent loci of membrane permeabilization. In order to achieve a merged locus between two or more particles, we assume that the distances between them needs to be short. A separation of a few nanometers would cause overlapping heating zones and therefore probably better perforation (see Fig. 5). This can also be realized by high particle concentrations, but this would also be related to adverse effects. A high particle concentration and cell surface coverage would cause many loci of perforation, permanently disrupting the cell integrity. The silica-GNP-particles maintain single perforation points on the cell surface. The spatial overlapping of heating zones is one of the beneficial features of combining silica and gold nanoparticles. The absorption efficiency of the gold particles and bubble formation threshold might be changed as well due to the binding to the silica particles which provide a solid interface. However, the silica-GNP-particles do not enable cell type selectivity as conjugated particles would do, because their weights prohibits antibody mediated targeting.

4. Conclusion

In recent studies, gold nanoparticle mediated laser transfection proved to be an excellent tool for the delivery of biologically relevant molecules into cells. In particular, it is best suited for antisense molecules like siRNA and Morpholino [15–17]. However, it is limited in use of small gold particles (< 100 nm) for the perforation procedure as these do not sediment on applicable time scales. Yet, small particles might better fit to the laser parameters, due to a shift in the plasmon resonance wavelength and the absorption (see Table 2). One method to overcome this problem was demonstrated by Yao et al., who used antibody labeled gold nanoparticles of 30 nm [20]. However, this would always require appropriate epitopes on the cell membrane.

In this study, we describe a new procedure employing silica-GNP-particles for laser perforation. The surfaces of the silica particles are coated with gold nanoparticles of different sizes resulting in equal or better perforation efficiencies in contrast to previous published

#211586 - $15.00 USD Received 13 May 2014; revised 26 Jun 2014; accepted 27 Jun 2014; published 17 Jul 2014

results on gold nanoparticle mediated laser perforation with free gold nanoparticles (see Fig. 4 and 5). The number of silica-GNP-particles per cell is as low as about 10 particles per cell, which is comparable to the previous studies with free gold nanoparticles [15]. It is important to emphasize, that this new procedure shortens the incubation time from three hours to 30 min. In this time, sedimentation and unspecific attachment are achieved. Furthermore, high particle concentrations at localized perforation points are reached, which leads to overlapping of heat or bubble formation. These hotspots might positively influence perforation efficiency.

With any new procedure, a critical assessment of the related complications is necessary. With regards to gold nanoparticle mediated laser perforation using silica-GNP-particles, these are on par with the standard procedure. It is desirable to remove particles from the cells after the procedure, instead of passaging the cells until no particles remain. Hence, we would favor, that further studies concentrate on an improvement of the safety of the procedure, for example by using immobilized gold nanostructures. Further studies have to address this issue. Gold particles which get lost from the silica by time or mechanical stress might influence the cells. In particular, 4 nm particles might lead to cyto- and genotoxic effects as demonstrated for small particles sizes [32,33]. For these reasons, the possibly best particle configuration from this study is 15 nm gold nanoparticles with a ratio of 1:40 and concentration of 10 particles per cell, combining high efficiency and best particle safety.

In a final analysis, the findings of this study have great importance for the field of laser transfection. They pave the way to a more efficient, faster, and safe high-throughput procedure for routine usage. The next steps will be to immobilize particles by a similar procedure and to test larger silica particles in combination with cell sorting. Larger fluorescent silica particles might be separable through cell sorting after trypsinization. If the attachment to the cells is too strong, PEGylation of the particles could be tested. Furthermore, the procedure might also apply in plasmonic photothermal therapy with gold nanoparticles to achieve better heating through overlapping of heating zones and zones of bubble formation.

Acknowledgments

We wish to extend special thanks for funding to the German Research Foundation (DFG) and the REBIRTH Cluster of Excellence. SK receives funding by the Hannover Biomedical Research School (HBRS) within REBIRTH. The authors thank the staff of the Biomedical Imaging and Manipulation group for their interest and support. We owe sincere gratitude to Andrea Deiwick for her excellent technical assistance.

#211586 - $15.00 USD Received 13 May 2014; revised 26 Jun 2014; accepted 27 Jun 2014; published 17 Jul 2014